Modelling bird songs: Voice onset, overtones and registers

Zaccarelli, Ricardo; Elemans, Coen; Fitch, Tecumseh; Herzel, Hanspeter

Published in:
Acustica United with Acta Acustica

Publication date:
2006

Document Version
Submitted manuscript

ACTA ACUSTICA UNITED WITH ACUSTICA
Vol. 92 (2006) 741 – 748

Modelling Bird Songs: Voice Onset, Overtones and Registers

Riccardo Zaccarelli[1], Coen P.H. Elemans[2], W. Tecumseh Fitch[3], Hanspeter Herzel[1]
[1]: Institute for Theoretical Biology (ITB), Humboldt University, Invalidenstr. 43, D-10115 Berlin, Germany
[2]: Experimental Zoology Group, Wageningen University, P.O. Box 338, 6700 AH Wageningen, The Netherlands
[3]: School of Psychology, University of St. Andrews, St. Andrews, Fife, KY16 9AJ, Scotland

Summary
We analyze two symmetric two-mass models of the avian syrinx. Our first model applies to songbirds and is a rescaled version of the well-known human two-mass model. Our second model (trapezoidal model) introduces a smoother geometry and is used to simulate the ring dove (*Streptopelia risoria*) syrinx. Simulations show that both models exhibit self-sustained vibrations. We show that the occurrence of collisions and the intensity of harmonics depend strongly on the configuration of the syrinx. The songbird model does not present instabilities. The trapezoidal model, however, displays coexisting limit-cycles that represent vibrations with, and without collisions at the same pressure. Register-like transitions are accompanied by subharmonics and deterministic chaos.

PACS no. 05.45.-a, 43.60.+d, 43.64.+r, 43.70.+i

1. Introduction

Two-mass models of mammalian vocal fold vibration have been used successfully to describe the normal voice [1, 2], vocal fold paralysis [3, 4, 5, 6], phonation onset [7], voice instabilities at high pressures [8] and source-tract coupling [9, 10].

In contrast to most mammals, birds do not generate vocalizations with their larynx but with their uniquely vocal organ, the syrinx [11]. Instead of vocal folds, thickened membranes called "labia" serve as vibrating tissue [12, 13, 14, 15]. However, sound production in birds is thought to be based on aerodynamical principles similar to that of human phonation [12, 13, 16]. Consequently, similar modelling approaches might be applicable and several types of biomechanical models have been developed [12, 16, 17, 18, 19]. It is not obvious that rescaling of the original two-mass model will lead to appropriate oscillations at realistic driving pressures and damping ratios. The syrinx is generally much smaller than the human larynx, which leads to smaller areas for the interactions between airflow and vibrating structures and to higher fundamental frequencies of the produced sound.

In this paper, we develop two biomechanical models of the syrinx to study the onset of sound generation and control of higher harmonics (overtones) in the absence of source-tract coupling.

Low-order models, as discussed in this paper, are oversimplifications of the physiology. More realistic geometries [2], additional degrees of freedom [20], coupling to the resonators [21] or a more detailed description of the jet separation [2] can improve the simulated sound signal significantly. In this paper we consider rather simple models with somewhat less realistic output. These core models allow comprehensive bifurcation analyses and we can address basic questions: Do we find reasonable vibrations of the masses even for much smaller geometries? How do symmetric upper and lower masses and a trapezoidal shape influence voice onset, spectral slope and voice instabilities?

In a first model version (rescaled two-mass model), we adapt the well-known simplified two-mass model to the dimensions of a songbird syrinx. Songbirds have two pairs of bilateral labia, which can operate as two independent sound sources [22]. Our model considers one unilateral pair of labia.

In the second model (trapezoidal model), a more realistic geometry of the so-called LTM (Lateral Tympaniform Membranes) is adopted to describe the syrinx of a non-songbird: the ring dove (*Streptopelia risoria*). The upper and lower masses are connected with massless plates on which pressure can act. Such a configuration with massless plates has been applied to reproduce experimental data from the human voice and to design laryngeal prostheses [21].

Both models exhibit self-sustained oscillations at physiologically realistic parameter values. In the classical two-mass model, as well as in the model of the songbird syrinx, collisions occur at medium pressures leading to strong harmonics. In the model of the dove syrinx, however, collision is partially avoided, leading to more pure

Received 25 January 2006,
accepted 27 June 2006.

tones. We relate these observations to the widely discussed topic of how birds control the intensity of their harmonics [23, 24, 25, 26, 27, 28, 29, 30]. The trapezoidal model exhibits coexisting vibratory regimes that resemble vocal registers. At the same subsyringeal pressure, vibrations with and without collisions are possible. Slow variation of subsyringeal pressure can induce subharmonics, deterministic chaos and a sudden jump to the other "registers".

2. The Models: Overview

Both models are governed by the same equations of motion:

$$\frac{\mathrm{d}x_1}{\mathrm{d}t} = v_1, \tag{1}$$

$$\frac{\mathrm{d}v_1}{\mathrm{d}t} = \frac{1}{m_1}\big(F_1 - r_1 v_1 - k_1 x_1 + I_1 - k_c(x_1 - x_2)\big), \tag{2}$$

$$\frac{\mathrm{d}x_2}{\mathrm{d}t} = v_2, \tag{3}$$

$$\frac{\mathrm{d}v_2}{\mathrm{d}t} = \frac{1}{m_2}\big(F_2 - r_2 v_2 - k_2 x_2 + I_2 - k_c(x_2 - x_1)\big), \tag{4}$$

where F_i are the pressure forces derived from the Bernoulli equation and the jet assumption and I_i represent the collision forces. We will give a detailed description of both models in the next sections.

3. Rescaled Two-mass Model

3.1. Derivation and voice onset

The classical two-mass model directly describes the well-known phase shift between upper and lower edge of aerodynamically driven vibrating tissue [31]. Originally, this model was derived in order to reproduce human vocal fold vibrations [1]-[10]. Therefore, it is not obvious that a rescaling of the original two-mass model will lead to appropriate oscillations at realistic driving pressures and damping ratios.

The fundamental frequency F_0 of many bird songs is on the order of 1 kHz. If we assume similar tissue elasticities (k_1, k_2) and density ρ as in human vocal fold modelling [1], we can derive the appropriate parameters of the rescaled model shown in Table I. We mantain the 5:1 ratio of lower to upper mass thickness (compare Figure 1).

The pressures are derived in earlier studies [5] from the Bernoulli equation using a jet assumption:

$$P_1 = P_s\left(1 - \Theta(a_{min})\left(\frac{a_{min}}{a_1}\right)^2\right)\Theta(a_1),$$

$$P_2 = 0,$$

where $\Theta(x)$ is the *Heaviside* function

$$\Theta(x) = \begin{cases} 1 & \text{if } x > 0, \\ 0 & \text{if } x \le 0. \end{cases}$$

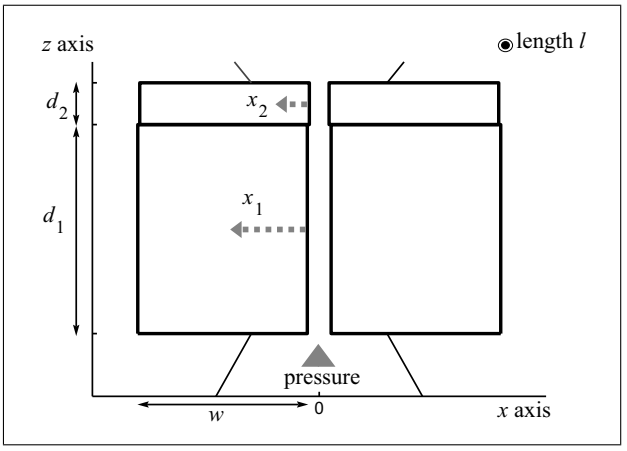

Figure 1. The rescaled two-mass model of the songbird syrinx.

Table I. Parameters of the rescaled two-mass model shown in Figure 1.

symbol	description	value
l	length of the syringeal lumen	0.3 cm
a_{01}	lower rest area	0.0021 cm^2
a_{02}	upper rest area	0.00175 cm^2
d_1	1^{st} mass thickness	0.1 cm
d_2	2^{nd} mass thickness	0.02 cm
m_1	1^{st} mass	0.0015 g
m_2	2^{nd} mass	0.0003 g
k_1	1^{st} mass stiffness	0.08 g/ms^2
k_2	2^{nd} mass stiffness	0.008 g/ms^2
r	damping constant ($r_1 = r_2$)	0.002 g/ms
k_c	coupling constant	0.025 g/ms^2

The forces F_i, I_i read as in previous studies [5]:

$$F_1 = l d_1 P_1, \tag{5}$$

$$F_2 = 0, \tag{6}$$

$$I_i = -\Theta(-a_i) c_i \frac{a_i}{2l}, \quad i \in \{1, 2\}. \tag{7}$$

Viscous resistance of the vibrating tissues can be expressed in terms of damping ratio $\zeta = r/2\sqrt{km}$ [1]. Because of the decreasing mass m, r was rescaled to keep approximately the same ζ values as in [1].

There is almost no information available on the prephonatory shape of vibrating tissues in avian phonation studies. Therefore, we have chosen rest areas a_{01} and a_{02} that allow easy vibrations, i.e. a low onset pressure. Systematic variations of the configuration revealed that a rectangular or a slightly convergent shape allow realistic onset pressures, close to the values reported in other models, e.g. [32].

Figure 2 shows the onset of self-sustained oscillations (solid Hopf bifurcation line) for increasing subsyringeal pressure P_s and varying stiffness k_1. The onset pressure of the rescaled model can be below 0.004 g/(cm ms^2) (400 Pascal $\approx$ 4 cm H_2O[1]) around our default parameters. Thus,

[1] All units are given in centimeters, grams and milliseconds and their corresponding combinations: hence pressure is measured in g/(cm ms^2)

rescaled dimensions with proper damping ratios and rest areas lead to an onset of oscillations at realistic pressure values. Therefore our rescaled two-mass model can serve as a first step to model vibrating tissues in the syrinx.

3.2. Intensity of overtones

The intensity of higher harmonics (overtones) is a widely discussed topic in bird song studies [23, 24, 25, 26, 27, 28, 29, 30]. A pure tone (e.g., a sine wave) has no overtones. Collisions of the vibrating tissues, however, lead to pronounced harmonics [31]. To study the intensity of overtones in the rescaled two-mass model, we calculate the power spectrum of the flow derivative $\frac{dU}{dt} = \dot{U}$ (we recall that $\dot{U}$ is a reasonable approximation of the radiated sound pressure [1]). We introduce a simple measure of the intensity of overtones - the *Harmonics Ratio* (HR):

$$HR = 10 \log \left(\frac{H_1}{H_0} \right),$$

which is calculated from the spectral power H_0 at the fundamental frequency and the power at the first harmonic, H_1. This quantity is closely related to the widely used spectral slope [31, 33]. Values below -20 dB indicate that the signal has weak overtones.

Figure 2 shows the values of HR (in grey scale) for varying subsyringeal pressure P_s and stiffness k_1. Only in the immediate neighborhood of phonation onset do nearly sinusoidal oscillations occur (e.g. at point A in Figure 2). Point B in Figure 2 represents a more typical situation: collisions of the masses lead to rather strong harmonics (Figure 3). In summary, the rescaled two-mass model can be used to model sound production with pronounced overtones. Extensive exploration of the effects of parameter variations revealed that the observed periodic vibrations with collision are quite robust. No register transitions or nonlinear phenomena such as subharmonics were found.

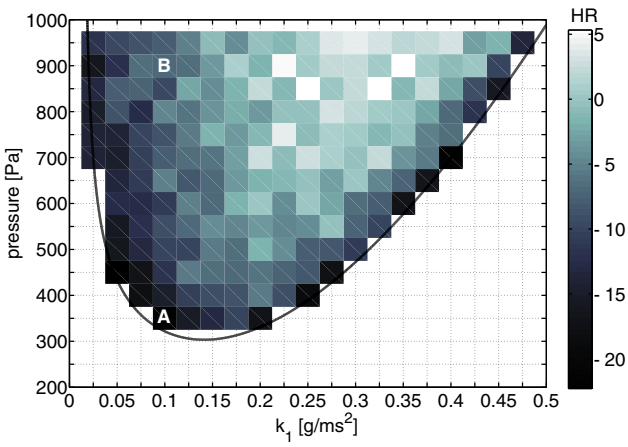

Figure 2. Variation of the onset pressure depending on the stiffness (solid Hopf bifurcation line) and Harmonic Ratio (HR) values color map above the onset of the pressure. At points A and B, i.e. close and relatively far away from the Hopf bifurcation, we evaluated the power spectrum of the flow derivative (see Figure 3). The fundamental frequencies at Ps=900 Pa range from approximately 800 Hz (k1 = 0.0025) to 2,400 Hz (k1=0.45).

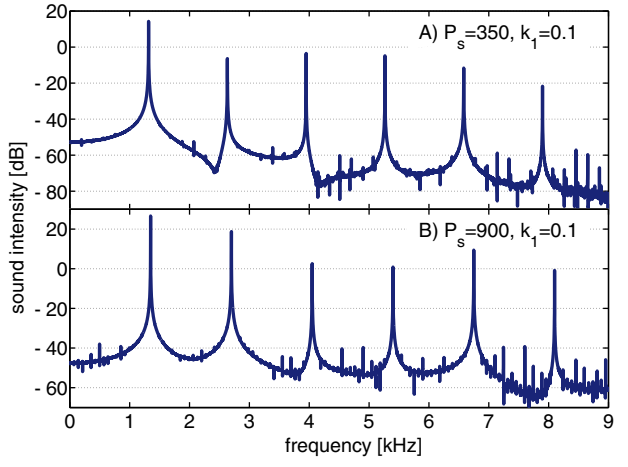

Figure 3. Power spectra at two different regimes corresponding to the letters A (upper panel) and B (lower panel, HR $\simeq$ -8) in Figure 2. Close to the Hopf bifurcation point (A) (Ps = 0.0035) we observe less intense harmonics (HR $\simeq -21$).

4. Trapezoidal Model

4.1. Geometrical aspects

In this section we will relax some over-simplifications of the original two-mass model along the lines of Refs. [2, 21]. The trapezoidal model aims to describe the syrinx of the ring dove (*Streptopelia risoria*). In contrast with songbirds, the vocal organ of ring doves is located at the bronchotracheal junction [34], i.e. above the bifurcation of the trachea into the bronchi. The anatomy of the ring dove syrinx (see Figure 4) suggests that a smoother model is more appropriate (*Streptopelia decaocto*, [35]; *Streptopelia risoria*, C.P.H. Elemans unpublished results). Therefore, each side of the LTM is modelled as a system of two masses linked together by three massless plates (see Figure 5), as presented in [21]. The parameters listed in Table II were obtained from anatomical studies (C.P.H. Elemans, unpublished results). Instead of the estimated total mass of approximately 9 mg, we assume a vibrating mass of 2 mg in order to achieve a reasonable fundamental frequency. Two important modifications of the two-mass model are introduced:

- symmetry between upper and lower masses (i.e. $m_1 = m_2, k_1 = k_2, r_1 = r_2$) as in [21], because there is no anatomical reason to introduce a small upper mass as in the classical two-mass model
- smoothed geometry via lower and upper plates which are characterized by the height parameters d_1 and d_3, respectively.

These modifications affect the calculation of pressure and collision forces significantly. For example, even for a closed syrinx there is a pressure force acting on the lower mass via the lower plate.

$= 10^5$ Pa. Consequently, with 1 cm $H_2O \approx 10^2 Pa$ we get 1 cm $H_2O \approx 0.001 g/(cm\,ms^2)$

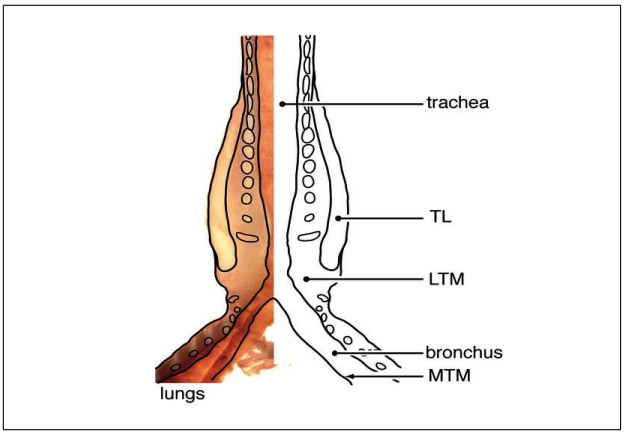

Figure 4. The syrinx of a ring dove (*Streptopelia risoria*). LTM: Lateral Tympaniform Membranes, MTM: Medial Tympaniform Membrane, TL: Tracheolateralis Muscle.

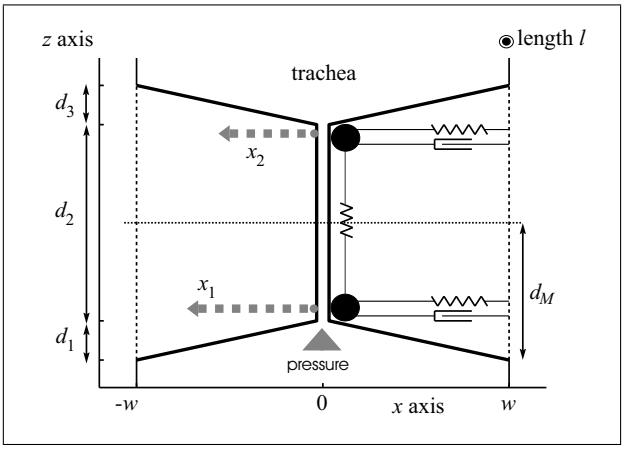

Figure 5. The model of the ring dove syrinx: the point masses are joined by three massless plates.

Table II. Parameters of the model of the ring dove syrinx (see Figure 5)

symbol	description	value
$2w$	width of the trachea	0.3 cm
l	length of the trachea	0.3 cm
a_{01}	lower rest area	0.003 cm^2
a_{02}	upper rest area	0.003 cm^2
d_1	1^{st} mass height	0.04 cm
$d_1 + d_2$	2^{nd} mass height	0.24 cm
$d_1 + d_2 + d_3$	LTM height	0.28 cm
m	masses ($m_1 = m_2$)	0.001 g
k	stiffness	0.02 g/ms^2
r	damping constant	0.001 g/ms
k_c	coupling constant	0.005 g/ms^2

4.2. Calculation of forces

In the traditional two-mass model, the area exposed to pressure (or collision) is always rectangular and normal to the motion of the masses [36]. In order to derive the pressure forces F_1, F_2, we need to multiply the pressure with the corresponding area. The collision forces I_1, I_2 can be written as a linear function of the areas a_1, a_2.

In our trapezoidal model, most of the quantities have to be generalized to adapt to the new model geometry. First, we assume for simplicity that all forces above the imaginary horizontal midline at $d_M = d_1 + \frac{d_2}{2}$ act on the upper mass whereas all forces below that midline drive the lower mass (midline assumption). Note that in Lous et al. [21], F_1 and F_2 are derived from a balance between forces and torques leading to a more detailed derivation of the force terms.

Second, we define the syringeal area at height z as $a(z) = 2lx(z)$, where $x(z)$ is obtained by means of plate equations, i.e. the linear equations which identify each plate on the plane xz. Particular values of $a(z)$ are a_1, a_2 (syringeal areas at 1^{st} and 2^{nd} mass heights, d_1 and d_1+d_2) and a_M (syringeal area at height d_M). The minimum syringeal area a_{min} is defined as $a_{min} = \min\{a_1, a_2\}$.

4.2.1. Pressure force

By means of the Bernoulli equation, jet separation assumption and $a(z)$ defined above, we can calculate the pressure $P = P(z)$ in the syringeal lumen at height z:

$$P(z) = \begin{cases} P_s\left[1 - \left(\frac{a_{min}}{a(z)}\right)^2\right]\Theta(z_m - z), & \text{if } a_{min} > 0, \\ P_s\Theta(\zeta_{min} - z), & \text{if } a_{min} \le 0, \end{cases}$$

where z_m is the ordinate at which a_{min} is found and, in case of collision ($a_{min} \le 0$), ζ_{min} is the minimum collision ordinate, i.e. the minimum ordinate z for which $a(z) \le 0$.

If z_0 and $z_1 (z_0 < z_1)$ are two generic ordinates of points belonging to the same plate and α the angle formed by that plate with the z axis, the pressure force acting on the plate area between z_0 and z_1 will be by definition $F(z_0, z_1) = \int_A P(z)dA$, where A is the plate area

$$A = \frac{z_1 - z_0}{\cos\alpha} l$$

Because no vertical motion is supposed, the component along the x axis of this pressure force reads:

$$\begin{aligned} F_x(z_0, z_1) &= \cos\alpha \; F(z_0, z_1) \\ &= \cos\alpha \int_0^{(z_1 - z_0)l/\cos\alpha} P(z)\,\mathrm{d}A = l\int_{z_0}^{z_1} P(z)\,\mathrm{d}z. \end{aligned}$$

Consequently, and by means of the midline assumption, the forces F_1, F_2 read:

$$F_1 = F_x(0, d_1) + F_x(d_1, d_M), \quad (8)$$

$$F_2 = F_x(d_M, d_2). \quad (9)$$

4.2.2. Collision force

Traditional two-mass models do not require the calculation of contact area, because the projected area is rectangular and there is no gradation in opening and closing [36]. We define a collision force that is consistent with (7) and admits a gradual variation of contact area in time. First, we remark that each collision force I_i is zero if:

$$I_i = 0 \Leftrightarrow a_i \ge 0 \text{ AND } a_M \ge 0, \quad i \in \{1, 2\}$$

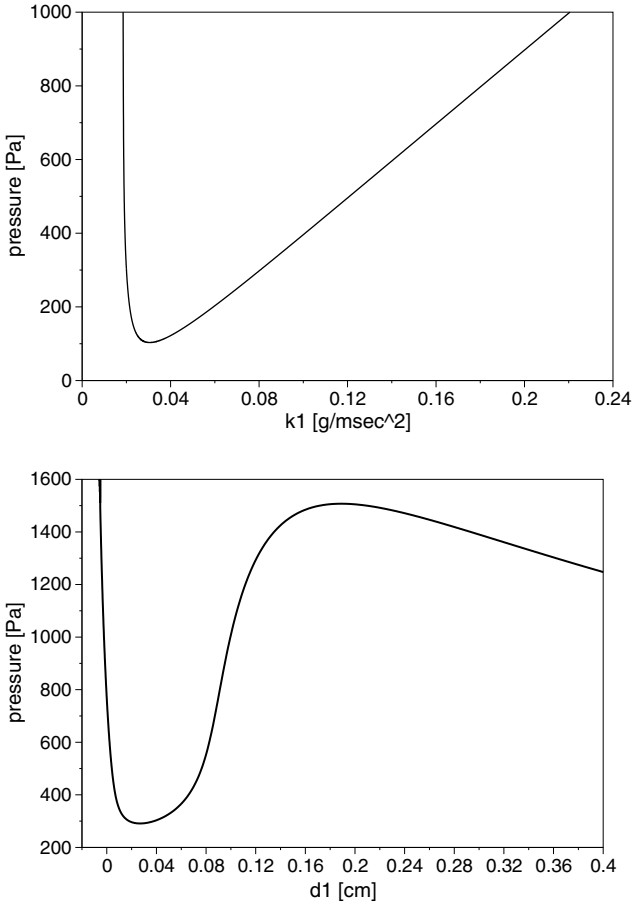

Figure 6. Onset pressure as a function of stiffness (upper graph) and of height d_1 (lower graph) for the trapezoidal model. Initial conditions: $[x_1, v_1, x_2, v_2] = [0, 0, 0, 0]$.

If the collision force I_i is nonzero, we define respectively:

$$I_1 = \frac{1}{\delta(0, d_M)} \int_0^{d_M} -\Theta(-a(z))a(z)\frac{c_i}{2l}\,\mathrm{d}z, \qquad (10)$$

$$I_2 = \frac{1}{\delta(d_M, d_3)} \int_{d_M}^{d_3} -\Theta(-a(z))a(z)\frac{c_i}{2l}\,\mathrm{d}z, \qquad (11)$$

where $\delta(z_1, z_2)$ is the distance (on the line $x = 0$) between z_1 and z_2 along which $a(z) < 0$.

We chose to normalize I_1 and I_2 using distance δ in order to keep c_i of the dimension of g/ms^2 and to obtain a generalization of the previous collision force. The latter is found comparing it with the degenerate case $d_1 = 0$. For the implementation of I_i, we take into account that the integrals in eq. (10) and (11) are proportional either to triangular or trapezoidal areas of colliding masses.

4.3. Bifurcations in the trapezoidal model

As in section 3.2, we study the onset of oscillations and the strength of harmonics in our trapezoidal model. The upper panel in Figure 6 shows that oscillations can be obtained at fairly low subsyringeal pressures (> 200 Pa). Increasing stiffness leads to an almost linear increase of the onset pressure as observed earlier in other models [5, 37]. An essential modification of the standard two-mass model is the

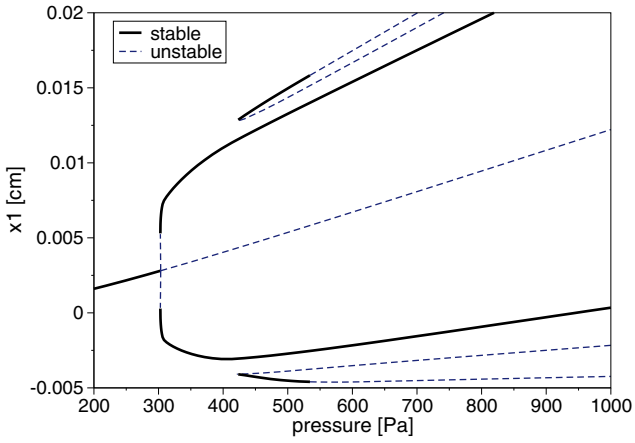

Figure 7. Bifurcation diagram of the variable x_1 for increasing subsyringeal pressure Ps. Note the coexistence of stable limit cycles around 450 Pa.

smoother geometry, i.e. a non-vanishing height d_1. It turns out that in a certain range around our default parameter (d_1 = 0.004 cm) oscillations are easily obtained (lower graph in Figure 6).

Figure 7 shows a one-dimensional bifurcation diagram for increasing subsyringeal pressure P_s. Figure 8 shows a more detailed bifurcation diagram near the onset visualizing coexisting limit cycles and negative values of the areas corresponding to colliding tissues. We observe in Figure 7 a sudden onset of oscillations around 300 Pa via a subcritical Hopf bifurcation. The amplitude of the resulting limit cycle increases and no collision occurs (see Figure 8). At 425 Pa another limit cycle with larger amplitudes is observed exhibiting collisions of the upper part described by x_2 (corresponding to negative values of a_2 in Figure 8). Furthermore, Figure 7 implies that quite distinct vibration patterns coexist at the same pressure. The large limit cycle contains stronger harmonics than the smaller one (Figure 9). These observations resemble observations in previous experiments of the chest to falsetto transitions in excised larynx studies [38]. Several register-like transitions were also found in simulations of an extended two-mass model [36]. Because the suppression of collision and the register transitions are novel features of our trapezoidal model, we discuss these phenomena in some detail.

4.4. Avoidance of collisions

As illustrated in Figure 2, the standard two-mass model is characterized by strong harmonics due to collision even at small and medium pressures. However, the lower limit cycle of our trapezoidal model is collision-free even at high pressures and consequently has only weak harmonics (lower panel in Figure 9). This is due to the increasing steady state area (see Figure 8) which pulls apart the masses. The equilibrium in the standard two-mass model, however, is constant, i.e. it does not depend on the subglottal pressure. If we set the derivatives with respect to time in the equations (1)–(4) to zero, we obtain in the two-mass model $x_2 = x_1\, k_c/(k_2 + k_c)$. For a rectangular

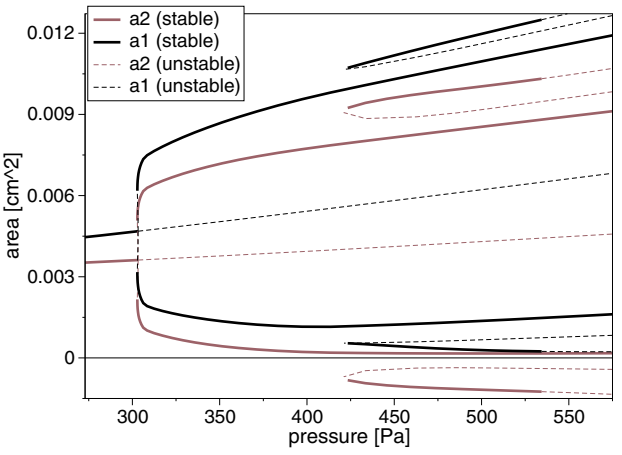

Figure 8. Detailed bifurcation diagram of the syringeal areas a_1, a_2 for increasing subsyringeal pressure Ps.

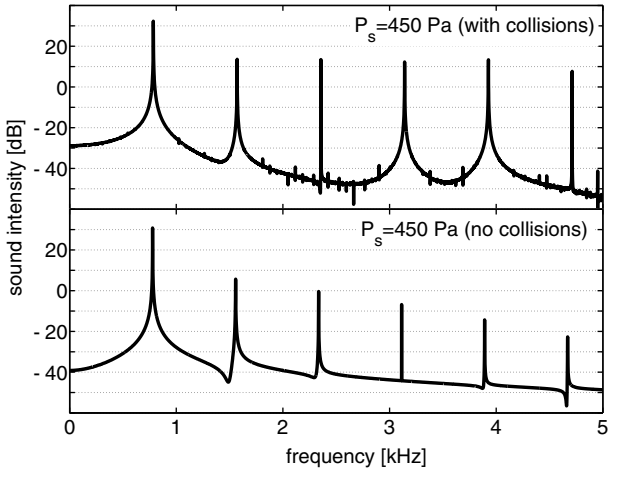

Figure 9. Power spectra at two different regimes: Collisions at larger vibrations lead to strong harmonics whereas harmonics decay rapidly for the small limit cycle.

shape ($a_{01} = a_{02} > 0$) we get from (2) the trivial solution $x_1 = x_2 = 0$. As shown in [5], oscillations starting from that rest position lead to collision, even for small pressures.

If we apply the same calculations to our trapezoidal model we obtain:

$$x_2 = \frac{k_c}{k_2 + k_c} x_1 + \frac{F_2}{k_2 + k_c}, \tag{12}$$

leading directly to

$$x_1 = \frac{(k_2 + k_c)F_1 + k_c F_2}{k_1 k_2 + k_1 k_c + k_2 k_c} > 0. \tag{13}$$

There is no simple analytical solution of this equation. However, because $F_1 > 0$ we get no equilibrium at $x_1 = x_2 = 0$. Therefore, the smoother geometry implies that there is always a force that pulls apart the masses, and the rest position increases linearly with the subsyringeal pressure (see Figure 7). Figure 8 shows that for the equilibria we always have $a_1 > a_2$, i.e. a convergent configuration.

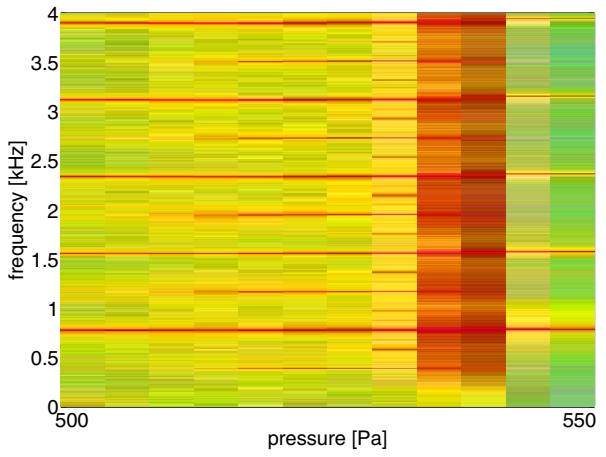

Figure 10. Register transitions from the large limit cycle to the small limit cycle (see Figure 7). Starting from a subsyringeal pressure of 500 Pa, we observe period doubling and chaos in the vicinity of the jump to the small limit cycle with less pronounced harmonics.

Because for a convergent shape the suprasyringeal pressure has little effect on the masses, such a persistent convergent configuration might lead to a reduced source-tract interaction.

It is clearly visible that both areas remain positive for the small limit cycle, while the large limit cycle exhibits negative values of a_2 corresponding to colliding tissues.

4.5. Register transitions via subharmonics and chaos

As described above, we found coexistence of a small and a large limit cycle in the range of 425-535 Pa. This implies that different initial conditions lead to distinct vibration patterns.

Furthermore, small perturbations can induce sudden jumps from one attractor to another. In this section we analyze the transition from the large attractor with collisions to the small limit cycle due to a slow increase of the subsyringeal pressure. Figure 10 shows the spectrogram of the sound pressure generated during the transition from the large limit cycle (with collisions) to the small limit cycle caused by a slow increase of the subsyringeal pressure. It is evident that there is a jump from harmonic rich spectra to a more sinusoidal oscillation.

Furthermore, subharmonics and noise-like components are visible. In Figure 11, high-resolution spectra[2] confirm the appearance of subharmonics and chaos. Using phase portraits and Poincaré sections (not shown), we have confirmed the existence of deterministic chaos in our trapezoidal model.

5. Discussion

Our simulations show that rescaled biomechanical models originally developed to describe mammalian vocal fold vi-

[2] Integration time from 1000 to 2000 ms in order to avoid transients and time step of 0.0005 msec (2000 kHz sampling rate).

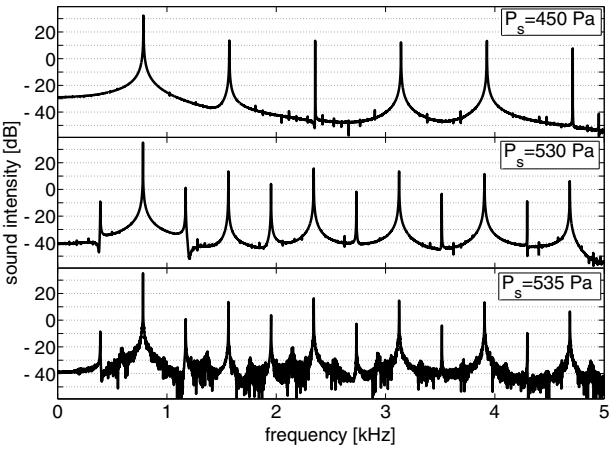

Figure 11. Power spectra at different pressure values for the large limit cycle depicted in Figure 7: As visible from the spectrogram in Figure 10, we detect a period doubling and chaos in the vicinity ($\simeq$ 540 Pascal) of the abrupt jump to the small limit cycle.

brations can be adapted to model the bird syrinx. We assumed that both sound producing organs are excited by the same principle: in the opening phase a high pressure drives the vibrating structure apart and during closure the pressure is reduced due to the Bernoulli force. The fundamental frequency is governed by the mass and stiffness of the vibrating tissue.

Our simulations represent symmetric vibrations. Interestingly, the same model equations can be used to model a single vibrating structure (a "hemi-syrinx"). In this case only the sound intensity is reduced but onset pressure or intensity of harmonics are identical.

Control of harmonics in bird songs is widely debated [23, 24, 25, 26, 27, 28, 29, 30]: some species have whistle-like songs and not much energy is found in the harmonics [26], whereas other species, such as the zebra finch (*Taenopygia guttata*), display strong harmonics during song or calls.

In all two-mass model versions almost pure tones are found near the onset of vibrations (i.e. near the Hopf bifurcation line shown in Figure 2). In the rescaled two-mass model, strong harmonics appear at higher pressures due to collisions. For a small upper mass and a rectangular geometry, collisions leading to strong harmonics can be avoided only near the phonation onset. At higher pressures counteracting forces would be required to diminish collisions. We hypothesize that the avoidance of strong collisions in song birds might be achieved by the medial tympaniform membranes (MTM) that are continuous with the inner vibrating labia [19]. This possible function of the MTM will be discussed in more details in a forthcoming study.

In our model of the ring dove syrinx no collisions occur at default parameters. Consequently, harmonics are fairly weak. The smoother configuration and equal upper and lower masses counteract collisions even at relatively high pressures. This is presumably due to a stronger effect of the subsyringeal pressure acting on both masses. In a recent experimental paper [23], Riede *et al.* showed how varying suprasyringeal configurations can suppress the second harmonic in ring doves, and Fletcher *et al.* [29] showed that the combined influence of trachea, glottis and upper esophagus acts as an effective band-pass filter that eliminates higher harmonics generated by the dove syrinx. Our simulations reveal that the configuration of the syrinx influences the intensity of overtones. Therefore, the amount of energy in the harmonics could also be controlled by syringeal muscles that directly affect the configuration of the syrinx [39, 40].

Around our default parameters given in Table I we found no voice instabilities. On the other hand, we have shown that our trapezoidal model exhibits coexistence of attractors and jumps from harmonic rich spectra to more sinusoidal oscillations of the radiated sound pressure.

A previously published two-mass model of the songbird syrinx [12] demonstrated many instabilities such as period doublings, transitions from periodic to chaotic dynamics, as well as mode locking transitions. Unfortunately, we are unable to compare the behaviour of the two models in more details, because the governing equations and the parameter settings were not provided. Ring doves already exhibit stronger harmonics during inspiratory phonation compared to expiratory phonation even at low intensities [23, 27, 41, 42]. This implies that asymmetries between outflow and inflow of the air have to be taken into account. This will be treated in a more sophisticated model. Instabilities such as frequency jumps are commonly observed in the ring dove coo [43, 41]. Even our current model described in this paper exhibits already coexistence of different "registers".

In this paper we have shown that the geometry and the rest position of the syrinx can influence the harmonic spectra drastically. Our simulations are a first step towards more realistic modelling of the syrinx. In subsequent studies we will incorporate the MTM and the dynamic control of associated superfast syringeal muscles. This will allow a quantitative comparison of observed bird songs and simulations.

Acknowledgements

The authors would like to thank two anonymous reviewers for their comments to improve the manuscript. We acknowledge support from the Deutsche Forschungsgemeinschaft (grant He 2168/7).

References

[1] K. Ishizaka, J. L. Flanagan: Synthesis of voiced sounds from a two-mass model of the vocal cords. Bell. Syst. Tech. J. **51** (1972) 1233–1268.

[2] X. Pelorson, A. Hirschberg, R. R. V. Hassel, A. P. J. Wijnands, Y. Auregan: Theoretical and experimental study of quasisteady-flow separation within the glottis during phonation. application to a modified two-mass model. J. Acoust. Soc. Am. **96** (1994) 3416–3431.

[3] N. Isshiki, M. Tanabe, M. Sawada: Arytenoid adduction for unilateral vocal cord paralysis. Arch. Otolaryngol. **104** (1978) 555–558.

[4] M. E. Smith, G. S. Berke, B. R. Gerrat, J. Kreiman: Laryngeal paralyses: Theoretical considerations and effects on laryngeal vibration. J. Speech. Hear. Res. **35** (1992) 545–554.

[5] I. Steinecke, H. Herzel: Bifurcations in an asymmetric vocal-fold model. J. Acoust. Soc. Am. **97** (1995) 1874–1884.

[6] P. Mergell, H. Herzel, I. R. Titze: Irregular vocal fold vibration - high-speed observation and modeling. J. Acoust. Soc. Am. **108** (2000) 2996–3002.

[7] P. Mergell, H. Herzel, T. Wittenberg, M. Tigges, U. Eysholdt: Phonation onset: vocal fold modeling and high-speed glottography. J. Acoust. Soc. Am. **104** (1998) 464–470.

[8] J. J. Jiang, Y. Zhang, J. Stern: Modeling of chaotic vibrations in symmetric vocal folds. J. Acoust. Soc. Am. **110** (2001) 2120–2128.

[9] P. Mergell, H. Herzel: Modelling biphonation - the role of the vocal tract. Speech Communication **22** (1997) 141–154.

[10] H. Hatzikirou, H. H. W. T. Fitch: Voice instabilities due to source-tract interactions. Acta Acustica united with Acustica **92** (2006) 468–475.

[11] C. H. Greenewalt: Bird song: Acoustics and physiology. Smithsonian Institution Press, Washington, D. C., 1968.

[12] M. S. Fee, B. Shraiman, B. Pesaran, P. P. Mitra: The role of nonlinear dynamics of the syrinx in the vocalization of a songbird. Nature **395** (1998) 67–71.

[13] F. Goller, O. N. Larsen: A new mechanism of sound generation in songbirds. Proc. Natl. Acad. Sci. USA **94** (1997) 14787–14791.

[14] O. N. Larsen, F. Goller: Role of syringeal vibrations in bird vocalisations. Proc. Roy. Soc. Lond.B. **266** (1999) 1609–1615.

[15] O. N. Larsen, F. Goller: Direct observation of syringeal muscle function in songbirds and a parrot. J. Exp. Biol. **205** (2002) 25–35.

[16] G. B. Mindlin, R. Laje: The physics of birdsong. Springer, Heidelberg, Germany, 2005.

[17] C. P. H. Elemans, O. N. Larsen, M. R. Hoffmann, J. L. Leeuwen: Quantitative modeling of the biomechanics of the avian syrinx. Animal Biol. **53** (2003) 183–193.

[18] N. H. Fletcher: Bird song: A quantitative acoustic model. J. Theor. Biol. **135** (1998) 455–481.

[19] M. S. Fee: Measurement of the linear and nonlinear mechanical properties of the oscine syrinx: Implications for function. J. Comp. Physiol. A. **188** (2002) 829–839.

[20] B. H. Story, I. R. Titze: Voice simulation with a body-cover model of the vocal folds. J. Acoust. Soc. Am. **97** (1995) 1249–1260.

[21] N. J. C. Lous, G. C. Hofmans, R. N. J. Veldhuis, A. Hirschberg: A symmetrical two-mass vocal-fold model coupled to vocal tract and trachea, with application to prosthesis design. Acta Acustica **84** (1998) 1135–1150.

[22] R. A. Suthers: Contributions to birdsong from the left and right sides of the intact syrinx. Nature **347** (1990) 473–477.

[23] T. Riede, G. J. L. Beckers, W. Blevins, R. A. Suthers: Inflation of the esophagus and vocal tract filtering in ring doves. J. Exp. Biol. **207** (2004) 4025–4036.

[24] D. H. Klatt, R. A. Stefanski: How does a mynah bird imitate human speech? J. Acoust. Soc. Am. **55** (1974) 822–832.

[25] S. Nowicki: Vocal tract resonances in oscine bird sound production: evidence from birdsongs in a helium atmosphere. Nature **325** (1987) 53–55.

[26] S. Nowicki, P. Marler, A. Maynard, S. Peters: Is the tonal quality of birdsongs learned? Ethology **90** (1992) 225–235.

[27] G. J. L. Beckers, R. A. Suthers, C. ten Cate: Pure-tone birdsong by resonance filtering of harmonic overtones. Proc. Natl. Acad. Sci. USA **100** (2003) 7372–7376.

[28] G. J. L. Beckers, B. S. Nelson, R. A. Suthers: Vocal-tract filtering by lingual articulation in a parrot. Current Biology **14** (2004) 1592–1597.

[29] N. H. Fletcher, T. Riede, G. J. L. Beckers, R. A. Suthers: Vocal tract filtering and the "coo" of doves. J. Acoust. Soc. Am. **116** (2004) 3750–3756.

[30] H. Williams, J. Cynx, F. Nottebohm: Timbre control in zebra finch (*Taeniopygia guttata*) song syllables. J. Comp. Psychol. **103** (1989) 366–380.

[31] I. R. Titze: Principles of voice production. Prentice-Hall, Englewood Cliffs, 1994.

[32] R. Laje, G. B. Mindlin: Modeling source-source and source-filter acoustic interaction in birdsong. Physical Review E **72** (2005) 1–11.

[33] D. Sciamarella, C. D'Alessandro: Stylization of glottal-flow spectra produced by a mechanical vocal-fold model. Proc. of the 9th European Conference on Speech Communication and Technology, Interspeech (2005) 2149–2152.

[34] F. Goller, O. N. Larsen: *In situ* biomechanics of the syrinx and sound generation in pigeons. J. Exp. Biol. **200** (1997) 2165–2176.

[35] M. R. Ballintijn, C. ten Cate, E. W. Nuijens, H. Berkhoudt: The syrinx of the collared dove (*Streptopelia decaocto*): Structure, inter-individual variation and development. Netherlands Journal of Zoology **45** (1995) 455–479.

[36] D. Sciamarella, C. d'Alessandro: On the acoustic sensitivity of a symmetrical two-mass model of the vocal folds to the variation of control parameters. Acta Acustica united with Acustica **90** (2004) 746–761.

[37] P. Mergell, H. Herzel, W. T. Fitch: Modeling the role of nonhuman vocal membranes in phonation. J. Acoust. Soc. Am. **105** (1999) 2020–2028.

[38] D. A. Berry, H. Herzel, I. R. Titze, B. H. Story: Bifurcations in excised larynx experiments. J. Voice **10** (1996) 129–138.

[39] C. P. H. Elemans, L. Y. Spierts, U. K. Mueller, J. L. van Leeuwen, F. Goller: Superfast muscles control doves trill. Nature **431** (2004) 146–146.

[40] C. P. H. Elemans, L. Y. Spierts, M. Hendriks, H. Schipper, U. K. Mueller, J. L. van Leeuwen: Syringeal muscles fit the trill in ring doves (*Streptopelia risoria*)s. J. Exp. Biol. **209** (2006) 965–977.

[41] C. P. H. Elemans: How do birds sing? sound analysis - mechanical modelling - muscular control. PhD thesis, Experimental Zoology Group, Wageningen University (2004) 92–107.

[42] A. S. Gaunt, S. L. L. Gaunt, C. R. M.: Syringeal mechanism reassessed: evidence from *Streptopelia*. Auk **99** (1982) 474–494.

[43] G. J. L. Beckers, R. A. Suthers, C. ten Cate: Mechanisms of frequency and amplitude modulation in ring dove song. J. Exp. Biol. **206** (2003) 1833–1843.